2014

Evidence for Hysteretic Substrate Channeling in the Proline Dehydrogenaseand Δ^1-Pyrroline-5-carboxylate Dehydrogenase Coupled Reaction of Proline UtilizationA(PutA)

Michael A Moxley
University of Nebraska - Lincoln

Nikhilesh Sanyal
University of Nebraska-Lincoln, nikhilesh1@gmail.com

Navasona Krishnan
University of Nebraska - Lincoln

John J. Tanner
University of Missouri-Columbia, Columbia, MO

Donald F. Becker
University of Nebraska-Lincoln, dbecker3@unl.edu

Follow this and additional works at: http://digitalcommons.unl.edu/biochemfacpub

Part of the Biochemistry Commons, Biotechnology Commons, and the Other Biochemistry, Biophysics, and Structural Biology Commons

Evidence for Hysteretic Substrate Channeling in the Proline Dehydrogenase and Δ^1-Pyrroline-5-carboxylate Dehydrogenase Coupled Reaction of Proline Utilization A (PutA)*

Michael A. Moxley[‡]**, Nikhilesh Sanyal**[‡]**, Navasona Krishnan**[‡]**, John J. Tanner**[§¶]**, and Donald F. Becker**[‡1]

From the [‡]*Department of Biochemistry, University of Nebraska-Lincoln, Lincoln, Nebraska 68588 and the Departments of* [§]*Biochemistry and* [¶]*Chemistry, University of Missouri-Columbia, Columbia, Missouri 65211*

Background: PutA from *Escherichia coli* is a bifunctional enzyme and transcriptional repressor in proline catabolism.
Results: Steady-state and transient kinetic data revealed a mechanism in which the two enzymatic reactions are coupled by an activation step.
Conclusion: Substrate channeling in PutA exhibits hysteretic behavior.
Significance: This is the first kinetic model of bi-enzyme activity in PutA and reveals a novel mechanism of channeling activation.

PutA (proline utilization A) is a large bifunctional flavoenzyme with proline dehydrogenase (PRODH) and Δ^1-pyrroline-5-carboxylate dehydrogenase (P5CDH) domains that catalyze the oxidation of L-proline to L-glutamate in two successive reactions. In the PRODH active site, proline undergoes a two-electron oxidation to Δ^1-pyrroline-5-carboxylate, and the FAD cofactor is reduced. In the P5CDH active site, L-glutamate-γ-semialdehyde (the hydrolyzed form of Δ^1-pyrroline-5-carboxylate) undergoes a two-electron oxidation in which a hydride is transferred to NAD$^+$-producing NADH and glutamate. Here we report the first kinetic model for the overall PRODH-P5CDH reaction of a PutA enzyme. Global analysis of steady-state and transient kinetic data for the PRODH, P5CDH, and coupled PRODH-P5CDH reactions was used to test various models describing the conversion of proline to glutamate by *Escherichia coli* PutA. The coupled PRODH-P5CDH activity of PutA is best described by a mechanism in which the intermediate is not released into the bulk medium, *i.e.*, substrate channeling. Unexpectedly, single-turnover kinetic experiments of the coupled PRODH-P5CDH reaction revealed that the rate of NADH formation is 20-fold slower than the steady-state turnover number for the overall reaction, implying that catalytic cycling speeds up throughput. We show that the limiting rate constant observed for NADH formation in the first turnover increases by almost 40-fold after multiple turnovers, achieving half of the steady-state value after 15 turnovers. These results suggest that *Ec*PutA achieves an activated channeling state during the approach to steady state and is thus a new example of a hysteretic enzyme. Potential underlying causes of activation of channeling are discussed.

The amino acid proline is of considerable interest because of its role in multiple processes such as cellular bioenergetics,

redox homeostasis, stress response, osmoprotection, and bacterial pathogenesis (1–3). Proline metabolism also influences apoptotic and cell survival signaling pathways that impact different processes such as tumorigenesis in mammals and, in worms, lifespan extension (4–6). These connections have led proline to be termed as a multifunctional amino acid and motivate the study of its metabolism (1).

The central pathway of proline catabolism is the four-electron oxidation of proline to glutamate catalyzed in a consecutive reaction by the enzymes proline dehydrogenase (PRODH)[2] and Δ^1-pyrroline-5-carboxylate (P5C) dehydrogenase (P5CDH) (Fig. 1). A defining feature of PRODH and P5CDH enzymes in different organisms is whether they are encoded separately or as a bifunctional enzyme known as PutA (proline utilization A; Fig. 2A) (7). Thus far, PutA enzymes have been found exclusively in Gram-negative bacteria, whereas separate PRODH and P5CDH enzymes occur in Gram-positive bacteria and eukaryotes. Certain PutAs also contain a DNA-binding domain such as the PutAs from *Escherichia coli* (Fig. 2A) and *Salmonella typhimurium* (7). In *E. coli*, PutA is the major regulator of the *put* regulon, which consists of the *putA* and *putP* genes that encode for PutA and the high affinity proline/Na$^+$ symporter PutP, respectively (8, 9). During periods of low proline availability, PutA represses the *put* regulon by binding to *putA/P* promoter regions (9). When high concentrations of proline are present, PutA repression is relieved by proline reduction of the FAD cofactor, which induces PutA binding to the inner cytoplasmic membrane, a process known as redox functional switching (8, 10, 11).

The covalent linking of enzymes catalyzing sequential reactions in a metabolic pathway, as in PutA, suggests the possibility of substrate channeling, *i.e.*, the intermediate species between the two reactions does not equilibrate with the bulk medium. The overall PutA reaction involves the intermediate P5C, which spontaneously hydrolyzes and equilibrates with L-gluta-

[2] The abbreviations used are: PRODH, proline dehydrogenase; CoQ$_1$, ubiquinone-1; GSA, L-glutamate-γ-semialdehyde; P5C, Δ^1-pyrroline-5-carboxylate; P5CDH, Δ^1-pyrroline-5-carboxylate dehydrogenase; SSE, sum square error.
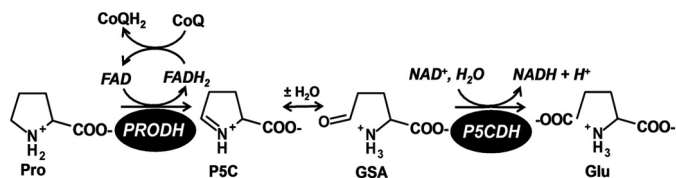
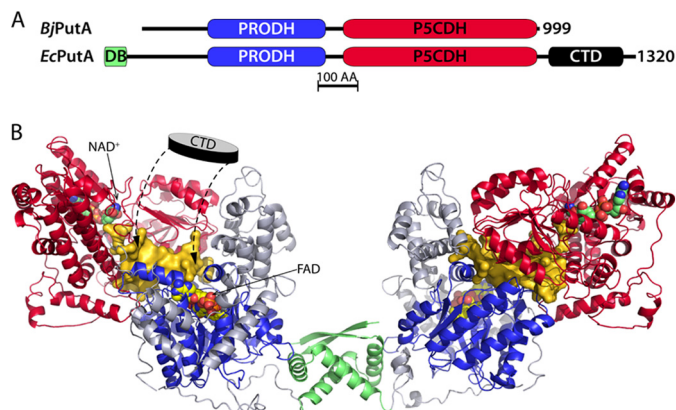FIGURE 1. **Reactions catalyzed by the PRODH and P5CDH domains of PutA.**

FIGURE 2. **EcPutA structural model.** *A*, domain diagrams for the small PutA from *B. japonicum* (*Bj*PutA) and the trifunctional PutA from *E. coli* (*Ec*PutA). *B*, model of the *Ec*PutA dimer from reference (20), which is based on small angle x-ray scattering, crystal structures of *Ec*PutA DNA-binding and PRODH domains, and homology to *Bj*PutA. The DNA-binding, PRODH, and P5CDH domains are colored as in the domain diagram. The gold surface represents the substrate-channeling cavity. The C-terminal domain (*CTD*), whose structure is unknown, is depicted as a lid that covers the substrate-channeling cavity.

mate-γ-semialdehyde (GSA) (Fig. 1). Recently, kinetic studies established that the P5C/GSA intermediate is channeled between the PRODH and P5CDH domains in PutA from *Bradyrhizobium japonicum* (*Bj*PutA) (12). Correspondingly, the x-ray crystal structure of *Bj*PutA revealed an internal cavity spanning 41 Å that connects the N-terminal PRODH domain to the C-terminal P5CDH domain. Also, PutA from *S. typhimurium*, which has 95% sequence similarity with *Ec*PutA, has been proposed to utilize a channeling mechanism (13, 14). The physiological benefit of channeling P5C/GSA is to prevent its potentially harmful reactions with other molecules and to avoid a futile cycle between proline catabolism and biosynthesis pathways, which share P5C/GSA as a common intermediate (15).

Although kinetic data for two PutAs are consistent with substrate channeling, the detailed mechanism of substrate channeling has not been determined. Thus, the aim of this study is to provide the first kinetic model of the coupled PRODH-P5CDH reaction in PutA. *Ec*PutA was chosen for this study because we previously determined the kinetic mechanism of the PRODH domain by steady-state (16) and rapid reaction (17) kinetic methods. *Ec*PutA PRODH catalyzes the oxidation of proline to P5C by a two-site ping-pong mechanism using the ubiquinone analog CoQ$_1$ as an electron acceptor. Stopped flow methods demonstrated that the oxidative half-reaction with CoQ$_1$ is rate-limiting in the PRODH reaction (17). Although the kinetic mechanism of the P5CDH domain has yet to be fully characterized in *Ec*PutA, it likely follows an ordered ternary mechanism as described for human P5CDH (18, 19).

*Ec*PutA was also chosen for this study because it is the archetype of trifunctional PutAs—those that function as both bifunctional enzymes and transcriptional repressors. Trifunctional PutAs are larger than the strictly bifunctional PutAs, such as *Bj*PutA, mainly because of an N-terminal ribbon-helix-helix domain (47 residues) used for DNA binding and a 200-residue C-terminal domain of unknown function (Fig. 2*A*). Although an x-ray crystal structure of full-length *Ec*PutA is not available, a model of *Ec*PutA (Fig. 2*B*) was recently constructed using the crystal structures of the PRODH and DNA-binding domains, a homology model of the P5CDH domain, and small angle x-ray scattering data of full-length *Ec*PutA (20). Interestingly, the small angle x-ray scattering data showed that *Ec*PutA and *Bj*PutA have completely different oligomeric states and quaternary structures, which results from the additional DNA-binding and C-terminal domains of *Ec*PutA. Nevertheless, the model predicts that the substrate-channeling cavity found in *Bj*PutA is conserved in *Ec*PutA (Fig. 2*B*). The C-terminal domain of *Ec*PutA, whose structure is unknown, is proposed to form a lid that helps seal the cavity from the outside environment (Fig. 2*B*); an oligomerization domain forms this lid in BjPutA.

Here we establish that the coupled PRODH-P5CDH activity in *Ec*PutA is best explained by a channeling mechanism. We also identify a limiting rate constant for the overall PRODH-P5CDH reaction that represents the channeling step of the mechanism. Furthermore, we show evidence of hysteresis in *Ec*PutA with a significant rate enhancement in the proposed channeling step upon subsequent enzyme turnover. This is the first kinetic modeling of the overall PutA reaction and provides a foundation for testing channeling mechanisms in other PutA enzymes.

EXPERIMENTAL PRODCEDURES

Materials—All chemicals and buffers were purchased from Fisher Scientific and Sigma-Aldrich. *E. coli* strains XL-Blue and BL21(DE3) pLysS were purchased from Novagen. PutA was expressed and purified with a N-terminal His$_6$ tag as previously described (21), including an additional anion exchange chromatography step (17), and stored at -80 °C. The concentration of PutA was determined using a molar extinction coefficient of 12,700 M^{-1} cm^{-1} at 451 nm (22). The *Ec*PutA mutants R556M and C917A were generated using the site-directed mutagenesis kit from Stratagene and purified according to the same protocol as WT *Ec*PutA described above.

(DL)-P5C (50/50 mixture) was synthesized by the method of Williams and Frank (23) and stored in 1 M HCl at 4 °C and was neutralized the day of experiments on ice by titrating with 6 M NaOH. Assays containing exogenously added (DL)-P5C contained ~150 mM NaCl from the pH neutralization. All experiments were conducted in Nanopure water.

Kinetic Experiments and Simulations—All kinetic experiments were performed on a stopped flow mixer (Hi-Tech SF-61DX2) at 21 °C. Experiments that are described as anaerobic were subjected to vacuum/nitrogen gas cycles followed by the addition of protocatechuate dioxygenase (0.05 unit/ml) and protocatechuic acid (100 μM) to scrub the remaining oxygen as described previously (17).

All kinetic experiments were analyzed using KinTek explorer software, which simulates experimental data by numerical integration of the rate equations using known initial conditions and then extracts kinetic parameters through global fitting of multiple data sets (24). All plots were made using Matlab 2011b software (Mathworks).

Stopped Flow Monitored NAD$^+$ Binding—The binding of increasing concentrations of NAD$^+$ to *Ec*PutA (2 μM after mixing) were followed by monitoring the quenching of *Ec*PutA tryptophan fluorescence excited at 280 nm where the emission was collected using a photomultiplier tube and filtered so that only emission past 310 nm was collected. Experiments were conducted in 50 mM potassium phosphate (pH 7.5) and 1 mM EDTA.

Kinetic traces were analyzed by fitting to a simple binding mechanism of one association/dissociation step using KinTek Explorer software. Equilibrium points were also analyzed by fitting to a rectangular hyperbola.

Steady-state P5CDH Assays—P5CDH assays were conducted in 50 mM potassium phosphate (1 mM EDTA, pH 7.5) using 0.25 μM *Ec*PutA and varying NAD$^+$ concentrations (0.5–500 μM) at different fixed concentrations of (DL)-P5C (0.125–2.7 mM). Progress of the reaction was followed by monitoring the formation of NADH ($\epsilon_{340\ nm} = 6.2\ mM^{-1}\ cm^{-1}$). The data were analyzed by globally fitting combined steady-state progress curves and single-turnover P5CDH data as described below.

P5CDH Single-turnover Experiments—P5CDH single-turnover experiments were conducted in the same buffer conditions as the steady-state P5CDH assays. *Ec*PutA (20 μM after mixing) was mixed with varying concentrations of NAD$^+$ (1–20 μM). The concentration of neutralized (DL)-P5C was fixed at 3.6 mM (1.8 mM L-P5C). The stopped flow data were globally fitted to an ordered ternary mechanism with initial velocity progress curves obtained from the P5CDH steady-state experiments.

Nonchanneling Simulations—Steady-state progress curves were simulated according to a ping-pong-type mechanism with rate constants for the *Ec*PutA PRODH domain determined previously (16, 17) and the ordered ternary mechanism for the P5CDH domain of *Ec*PutA described here. Simulations were produced with the same conditions used in steady-state channeling assays described below. The signal was considered to be enzyme-bound and free NADH.

EcPutA Single-turnover and Steady-state Channeling Experiments—Single-turnover and steady-state channeling experiments were performed in 50 mM K$^+$-phosphate (pH 7.5) with a final concentration of 25 mM NaCl and were followed by a photodiode array detector and at 340 nm using a photomultiplier tube. Single-turnover channeling experiments were performed under anaerobic conditions as described above and after mixing contained 0.2 mM NAD$^+$ and different concentrations of *Ec*PutA and proline.

Single-turnover experiments were analyzed by fitting the data to a single exponential equation and to a simulated mechanism accounting for PRODH domain activity as described (17). P5CDH activity was accounted for by a channeling step (first order step) intended to model the direct movement of the intermediate P5C/GSA from the PRODH active site to the P5CDH active site. It should be noted that P5C is assumed to rapidly and nonenzymatically convert to GSA, which is the actual substrate for the P5CDH reaction (25). The P5CDH active site is modeled as an ordered ternary mechanism and was kinetically constrained according to established rate constants from P5CDH activity alone as described in this study.

Anaerobic Multiple-turnover Experiments—*Ec*PutA and solutions were prepared anaerobically as described above in 50 mM K$^+$-phosphate (pH 7.5) with a final concentration of 25 mM NaCl. Experiments were followed using multiwavelength detection, and then single wavelength data were subsequently extracted. The first multiple-turnover experiment was intended to produce approximately five turnovers of PRODH-P5CDH coupled activity at equilibrium. This experiment contained 10 μM *Ec*PutA, 250 μM NAD$^+$, and 50 μM CoQ$_1$ with varying concentrations of proline (1–25 mM). The number of turnovers at equilibrium was approximated by dividing the concentration of the limiting reagent (CoQ$_1$) by the enzyme concentration.

The second multiple-turnover experiment was intended to produce ~25 turnovers of PRODH-P5CDH coupled activity at equilibrium. This experiment contained a final concentration of 2 μM *Ec*PutA (concentration after mixing) with the same concentrations of the other reagents mentioned above for the first multiple-turnover channeling experiment.

Simulation of Time-dependent Activation of EcPutA Channeling—Simulations were performed with 0.5 μM *Ec*PutA, 10 mM proline, 0.3 mM CoQ$_1$, and 0.2 mM NAD$^+$. The sum of all activated and inactivated *Ec*PutA species were treated as separate signals and normalized according to the total *Ec*PutA concentration. Product concentration was modeled as the sum of free and enzyme-bound NADH species. The linear portion (100–300 s) of the product concentration progress curve was fitted to a line to estimate the transient time (26, 27).

RESULTS

Stopped Flow Fluorescence Monitored Binding of NAD$^+$—A thorough kinetic description of the PRODH-P5CDH coupled reaction of PutA requires knowledge of the mechanisms and rate constants for the individual PRODH and P5CDH activities. Previously, we reported the kinetic mechanism for the PRODH domain of *Ec*PutA using both steady-state and rapid reaction methods (16, 17). Here, we provide analogous data for the P5CDH domain.

Microscopic rate constants for the association and dissociation of NAD$^+$ to the P5CDH domain of *Ec*PutA were determined with stopped flow protein fluorescence. *Ec*PutA was rapidly mixed with varying concentrations of NAD$^+$ and followed by exciting *Ec*PutA fluorescence at 280 nm (Fig. 3*A*). Varying concentrations of NAD$^+$ were shown to quench *Ec*PutA tryptophan fluorescence (Fig. 3*A*). The signal was fitted using KinTek software to a simple binding mechanism that only included association and dissociation steps.

NAD$^+$ binding was readily monitored by stopped flow so that well constrained rate constants for the association ($k_1 = 235\ mM^{-1}\ s^{-1}$) and dissociation ($k_{-1} = 2.13\ s^{-1}$) of NAD$^+$ were obtained (Fig. 3*B* and see Table 1 for confidence intervals). NAD$^+$ binding data were also fitted to single exponentials, and k_{obs} values were plotted against NAD$^+$ concentration as shown in Fig. 3*C*. The analytical fitting yielded rate constants of 226 mM^{-1} s^{-1} (k_1) and 2.24 s^{-1} (k_{-1}) and also indicated a simple binding mechanism. A plot of the amplitudes (Fig. 3*D*) yielded a
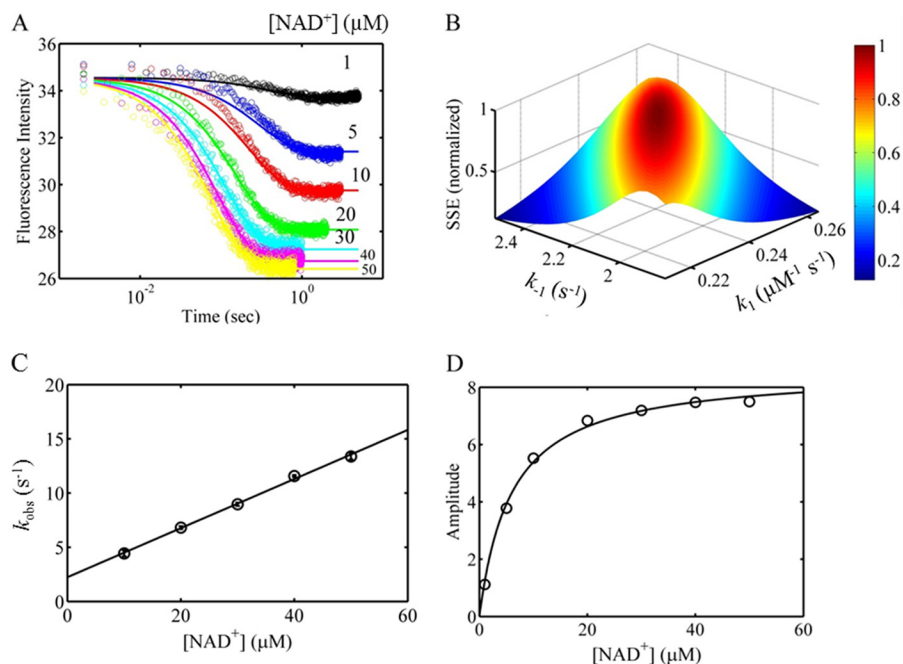
FIGURE 3. **Stopped flow kinetics of NAD$^+$ binding to *Ec*PutA.** *A*, *Ec*PutA (2 μM after mixing) was rapidly mixed with varying concentrations of NAD$^+$ (after mixing) as annotated and followed by *Ec*PutA fluorescence quenching (excited at 280 nm). *Circles* represent experimental data. *Solid curves* represent fits to a simple binding model that includes only association and dissociation steps. *B*, the FitSpace for the model of NAD$^+$ binding to *Ec*PutA. The *z* axis represents the SSE between the model and the data, normalized so that the best fit gives a value of 1 (30). Best fit values as well as confidence intervals are reported in Table 1. *C*, observed first order rate constants extracted from the data in *A* by fitting to a single exponential equation (NAD concentrations of 1 and 5 μM were omitted to adhere to pseudo first order conditions for analytical fitting). The linear fit assumes a simple binding model (55), yielding an association rate constant (k_1) of 0.226 μM^{-1} s^{-1} from the slope and a dissociation rate constant (k_{-1}) of 2.24 s^{-1} from the *y* intercept. *D*, amplitudes extracted from the data in *A* by fitting to a single exponential equation. The hyperbolic fit yields a dissociation constant (K_d) of 5 μM.

TABLE 1

Kinetic parameters for EcPutA P5CDH activity

The values are from global fitting to the mechanism shown in Fig. 5.

Parameter	Best fit value	Lower bound	Upper bound
k_1	235 mM^{-1}s^{-1}	215 mM^{-1}s^{-1}	257 mM^{-1}s^{-1}
k_{-1}	2.13 s^{-1}[a]	1.91 s^{-1}	2.39 s^{-1}
K_d (L-P5C/GSA)	2.9 mM^a		
k_3	7.67 s^{-1}	6.41 s^{-1}	9.94 s^{-1}
k_{-3}	0^b		

^{a} Boundaries for K_d values are not determined using KinTek software.
^{b} Fitting pushed the value for k_{-3} very low; thus k_{-3} was fixed at 0 for the final fitting. Furthermore, no reverse reaction was observed.

dissociation constant (K_d) of 5 μM, which is similar to the ratio of stopped flow rate constants of $k_{-1}/k_1 = 10$ μM.

Steady-state and Single-turnover P5CDH Kinetics—With the NAD$^+$ binding step now constrained, we next obtained kinetic constants for subsequent steps in the P5CDH reaction. Steady-state data for the P5CDH reaction were collected by monitoring the absorbance of NADH at 340 nm by varying NAD$^+$ concentration using different fixed concentrations of P5C/GSA (Fig. 4, *A–D*). In addition, single-turnover experiments were performed using 20 μM *Ec*PutA with varying concentrations of NAD$^+$ (1–20 μM) and a fixed concentration of P5C/GSA (Fig. 4*E*). In these experiments, enzyme-bound and free NADH were monitored. We tested the ability of *Ec*PutA to catalyze the reverse P5CDH reaction using NADH and glutamate, but no activity was detected in this direction. Furthermore, product inhibition of the P5CDH reaction was not observed with glutamate at concentrations up to 50 mM. Because product release cannot limit a single-turnover reaction, the observed rate constant is considered to be reporting on a chemical step.

Both steady-state and single-turnover P5CDH data were fitted together to an ordered ternary mechanism as shown in Fig. 5 with the binding steps for NAD$^+$ constrained by the kinetic constants determined above. Data were fitted only to a ternary mechanism because the hydride transfer step between GSA and NAD$^+$ requires a ternary complex. Because no activity was detected for the reverse P5CDH reaction, the fitted mechanism was simplified such that the chemical step was made irreversible as shown in Fig. 5. Our data do not yield specific information on the association and dissociation rate constants of the products except that their release is not rate-limiting. Thus, glutamate and NADH dissociation rates were considered to be fast. The individual rate constants (k_2 and k_{-2}) for L-P5C/GSA binding to the P5CDH domain were not well constrained; however, a K_d value of 2.9 mM was derived from global fitting (Table 1).

As shown in Fig. 4*F*, global fitting of the data revealed a well constrained rate constant of 7.67 s^{-1} for the chemical step (k_3; Fig. 5). A k_{cat} of 5.16 s^{-1} for the *Ec*PutA P5CDH reaction was calculated from our determined rate constants using the definition of k_{cat} from the kinetic mechanism shown in Fig. 5. Other calculated steady-state kinetic parameters for the P5CDH reaction are listed in Table 2. The best fit kinetic constants and confidence intervals for the P5CDH fitted mechanism are summarized in Table 1.

Evidence for Substrate Channeling in EcPutA—Transient time analysis, a classic test for substrate channeling, was applied to *Ec*PutA. The time-dependent production of NADH in an assay containing proline, CoQ$_1$, and NAD$^+$ was followed by monitoring absorbance at 340 nm. The progress curve does not
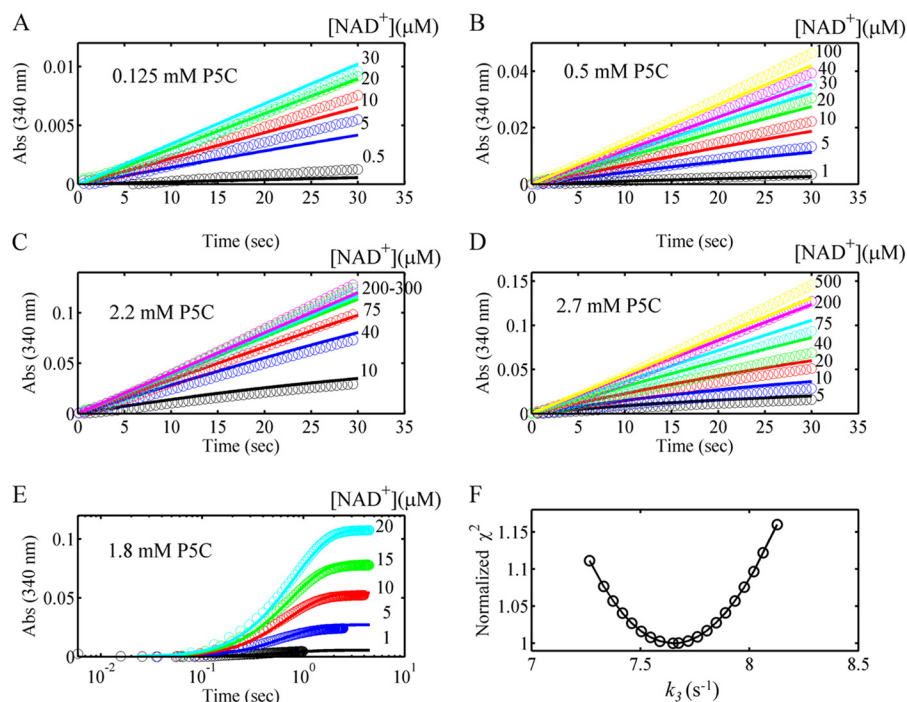
FIGURE 4. **Steady-state and single-turnover analysis of the P5CDH activity of *Ec*PutA globally fitted to an ordered ternary mechanism.** *A–D*, steady-state progress curves of *Ec*PutA P5CDH activity followed at 340 nm with varying NAD$^+$ concentrations at different fixed concentrations of exogenously added (DL)-P5C (L-P5C concentration shown). Experimental data are represented by *open circles*. The *solid curves* represent the results of global fitting of all the steady-state data and the single-turnover data shown in *E* to an ordered ternary mechanism (shown in Fig. 5). *E*, single-turnover progress curves of *Ec*PutA P5CDH activity followed at 340 nm. *Ec*PutA (20 μM after mixing) was rapidly mixed with varying concentrations of NAD$^+$ using a fixed concentration of exogenous (DL)-P5C (L-P5C, 1.8 mM). The experimental data are represented by *open circles*. The *solid curves* represent the results of global fitting of all the steady-state data from *A–D* along with the single-turnover data to an ordered ternary mechanism (Fig. 5). *F*, one-dimensional FitSpace (30) of the chemical step (k_3) from global fitting of the data in *A–E* to an ordered ternary mechanism, with the SSE normalized to one. The resulting best fit rate constants and confidence intervals are shown in Table 1.
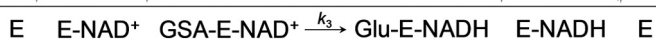

FIGURE 5. **Ordered ternary mechanism used for global fitting of the steady-state and single-turnover data of *Ec*PutA P5CDH activity with exogenous L-P5C/GSA.**

TABLE 2
Steady-state kinetic constants for EcPutA enzyme activities

Parameter	PRODH[a]	P5CDH[b,c]	PRODH-P5CDH[b]
k_{cat} (s^{-1})	5.2 ± 0.3	5.16	0.73 ± 0.1
K_m (pro) (mM)	42 ± 4	NA[d]	20.8 ± 2
k_{cat}/K_m (pro) (M^{-1} s^{-1})	123.8	NA	35 ± 5
K_m (P5C) (mM)	NA	2	NA
k_{cat}/K_m (P5C) (M^{-1} s^{-1})	NA	2.6	NA
K_m (NAD$^+$) (μM)	NA	22	23.5 ± 3
k_{cat}/K_m (NAD$^+$) (mM^{-1} s^{-1})	NA	235	31 ± 4

[a] Values were determined previously by following CoQ$_1$ reduction (16).
[b] Values are from assays following reduction of NAD$^+$.
[c] Values were calculated from fitted microscopic rate constants using steady-state constant definitions from the ordered ternary mechanism shown in Fig. 5.
[d] NA, not applicable.

show a lag phase (Fig. 6*A*), which is consistent with substrate channeling.

Nonchanneling control assays paralleling those developed in our studies of *Bj*PutA were also performed (12). In the control assay, *Ec*PutA is replaced by an equimolar mixture of two mutant *Ec*PutA enzymes deficient in either PRODH activity (R556M) or P5CDH activity (C917A). Arg-556 binds the carboxylate of proline in the PRODH site, and Cys-917 is the

nucleophile for the P5CDH reaction. We verified that R556M lacks PRODH activity (not shown) and retains full P5CDH activity (Fig. 6*D*). Likewise, C917A exhibits no P5CDH activity yet retains WT PRODH activity (Fig. 6*C*). The transient time assay for the mixture of mutants shows a significant lag corresponding to a transient time of ~5 min (Fig. 6*B*). This value is similar to the 7-min lag detected in nonchanneling control assays of *Bj*PutA (12).

Further insight was obtained by simulating progress curves using the kinetic constants and mechanisms for the individual *Ec*PutA PRODH (17) and P5CDH activities (Table 2). The nonchanneling coupled PRODH-P5CDH reaction was simulated according to the determined mechanisms of the PRODH (ping-pong (16, 17)) and P5CDH (ternary, described above) domains and corresponding rate constants using KinTek software. The simulations were produced in the given assay conditions and overlaid with data from WT *Ec*PutA (Fig. 6*A*) and the *Ec*PutA mixed variants (Fig. 6*B*). The fits were optimized to the nonchanneling model, allowing only minor changes in rate constants based on confidence intervals determined for WT *Ec*PutA PRODH and P5CDH domain activities. This analysis shows that WT *Ec*PutA coupled PRODH-P5CDH activity cannot be explained by a nonchanneling model (Fig. 6*A*). The simulated curve shows a pronounced lag, which differs substantially from the nearly linear experimental progress curve (Fig. 6*A*). In contrast, a simulated progress curve shows good agreement with the data for the mixed variants (Fig. 6*B*). This analysis suggests that the lag observed for the nonchanneling control rep-
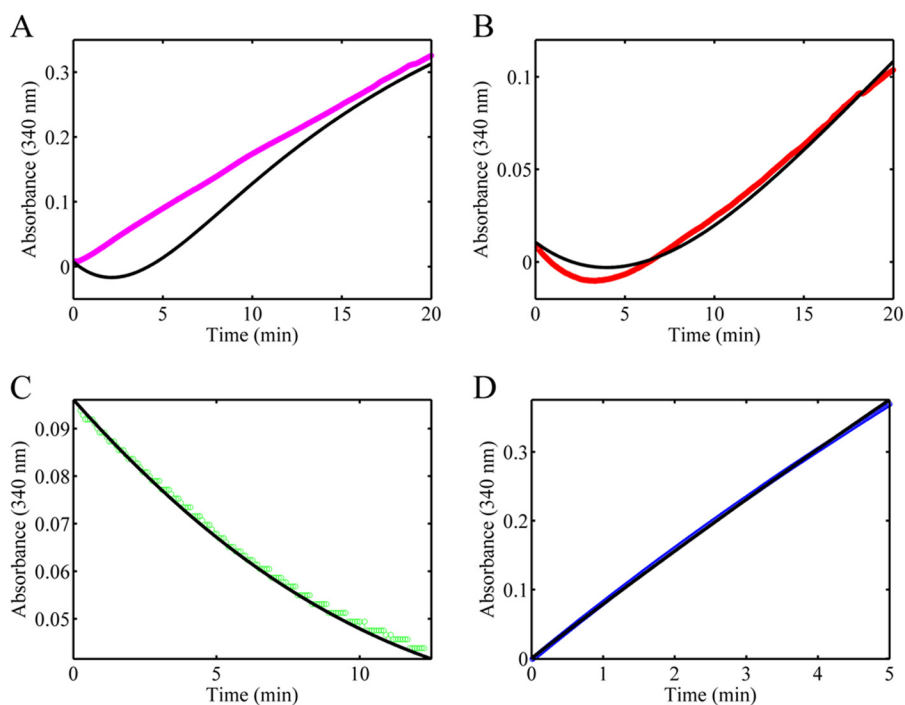
FIGURE 6. **Steady-state reaction progress curves of coupled PRODH and P5CDH activity for WT and mixed variant *Ec*PutA analyzed according to a nonchanneling mechanism.** *A*, steady-state assay of WT *Ec*PutA (0.5 μM) containing 0.1 mM CoQ$_1$, 0.2 mM NAD$^+$, and 40 mM proline followed at 340 nm (data in *magenta*). A simulated progress curve (*black line*) for a nonchanneling mechanism generated from rate constants determined previously for WT *Ec*PutA PRODH activity and P5CDH activity is also plotted (17). The poor fit of the data to the model is consistent with a substrate channeling mechanism for WT *Ec*PutA. *B*, steady-state assay containing equimolar amounts of the *Ec*PutA mutants R556M and C917A (0.2 μM), also referred to as mixed variants, with 0.1 mM CoQ$_1$, 0.2 mM NAD$^+$, and 40 mM proline followed at 340 nm (data in *red*). A simulated progress curve (*black line*) for a nonchanneling mechanism as described in *A* is also plotted (17). The good fit of the data to the model is consistent with a lack of substrate channeling for the mixed variants system. *C*, the *Ec*PutA mutant C917A was assayed for PRODH activity by following the reduction of CoQ$_1$ at 340 nm in the presence of 0.1 mM CoQ$_1$, 40 mM proline, and 0.2 μM C917A enzyme. Data (*green circles*) were plotted against a simulated progress curve (*black line*) using rate constants determined previously for WT *Ec*PutA PRODH activity (17). The excellent fit verifies that mutation of Cys-917 to Ala does not affect the PRODH activity. *D*, the *Ec*PutA mutant R556M was assayed for P5CDH activity by following the reduction of NAD$^+$ at 340 nm in the presence of 0.2 mM NAD$^+$, 0.6 mM L-P5C, and 0.2 μM R556M enzyme. The data (*blue circles*) were plotted against a simulated progress curve (*black line*) using rate constants determined here for WT *Ec*PutA P5CDH activity (Table 1). The excellent fit verifies that mutation of Arg-556 to Met does not affect the P5CDH activity.

resents the buildup of P5C/GSA in the bulk medium, and the absence of this diagnostic feature in the experimental WT progress curve suggests that substrate channeling occurs in *Ec*PutA.

Single-turnover Kinetics of the EcPutA PRODH-P5CDH Coupled Reaction—Stopped flow experiments with *Ec*PutA were then performed using single-turnover conditions to further examine substrate channeling in the PRODH-P5CDH coupled reaction. Single-turnover conditions were made by excluding CoQ$_1$ and performing the experiments anaerobically to eliminate interference by molecular oxygen as an alternative electron acceptor. *Ec*PutA and substrate solutions were made anaerobic and then rapidly mixed under anaerobic conditions on the stopped flow instrument. The reaction was followed by monitoring the UV-visible absorption spectrum (300–550 nm) using a photodiode array detector (Fig. 7*A*). A decrease in absorbance at 450 nm followed by an increase in absorbance at 340 nm was observed, indicating reduction of the FAD cofactor by proline and formation of NADH, respectively. Single wavelength data at 340 nm were extracted from the multiwavelength data set and used for analyzing the reaction. The data from different proline concentrations were fitted to a single exponential (single exponential fits not shown). The k_{obs} for the absorbance change at 340 nm decreases at proline concentrations of >10 mM (Fig. 7*B*), indicating substrate inhibition at high proline concentrations.

The data were then fitted to a model (Fig. 8) that includes a single intervening or channeling step between the PRODH (reductive half-reaction by proline) and P5CDH reactions. Because proline was observed to act as an inhibitor as described above, a dead-end inhibition step was also included in the mechanism. Single-turnover rate constants determined previously for the individual catalytic domains were used to constrain the fitting procedure. This analysis yields a best fit value of 0.037 s^{-1} for the channeling step rate constant in the first turnover (Fig. 7*C*). Changes in the normalized sum of square error (SSE) while the channeling rate constant is being varied are shown in the *inset* of Fig. 7*C*. This calculation shows that the rate constant for the proposed channeling step is well defined (confidence interval, 0.033–0.041 s^{-1}) given that the previously determined rate constants are fixed for the other obligatory steps in the overall reaction. The K_I for proline binding to the P5CDH active site was estimated to be 83 mM.

Evidence for Hysteresis in the EcPutA PRODH-P5CDH Reaction—The rate constant of 0.037 s^{-1} determined from best fit analysis of the single-turnover data in Fig. 7 is inconsistent with the steady-state k_{cat} of 0.733 s^{-1} for the overall *Ec*PutA coupled PRODH-P5CDH reaction (Table 2). The rate constant for the first turnover is ~20-fold slower than the steady-state turnover rate, which contradicts the corollary of enzyme kinetics that each forward obligatory first order step in the mecha-
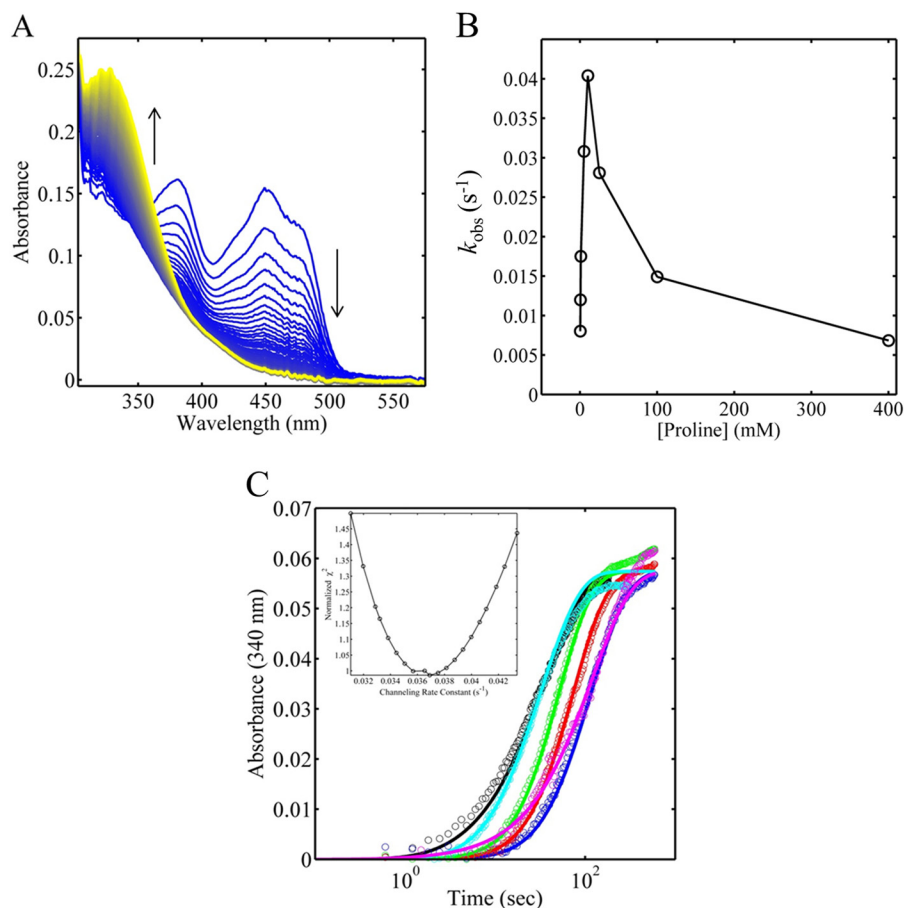
FIGURE 7. **Single-turnover experiment of *Ec*PutA coupled PRODH-P5CDH activity.** *A*, *Ec*PutA (12 μM after mixing) was rapidly mixed with 25 mM proline and 0.2 mM NAD$^+$ (concentrations after mixing) in anaerobic conditions, and absorbance changes were followed using a photodiode array detector. *B*, the observed first order rate constants obtained by fitting the absorbance at 340 nm from multiwavelength data of the coupled PRODH-P5CDH reaction at different proline concentrations to a single exponential equation (not shown). *C*, single wavelength traces at 340 nm from multiwavelength data of the coupled PRODH-P5CDH reaction at different proline concentrations were fitted to a channeling model (Fig. 8) using previously determined mechanisms and rate constants for *Ec*PutA PRODH activity (17) and P5CDH activity described here. Proline concentrations after mixing were 0.25 (*blue*), 0.5 (*red*), 1 (*green*), 5 (*black*), 25 (*cyan*), and 400 mM (*pink*), where data are shown as *colored circles*, and the predicted traces are represented by the corresponding *colored curves*. The *inset* shows a one-dimensional parameter scan of the channeling rate constant where the *y* axis is the normalized ratio χ^2/χ^2_{min} (30). Best fit rate constants and confidence intervals are reported in Table 3.

nism must have a rate constant higher than k_{cat}. This suggests that the rate constant in question, which represents substrate channeling, increases in subsequent turnovers during the approach to steady-state, a phenomenon known as enzyme hysteresis (28, 29).

To explore the possibility of hysteresis with *Ec*PutA, we first combined the single-turnover and steady-state kinetic data using a global fitting approach. To account for steady-state turnovers, the oxidative half-reaction with CoQ$_1$ was added for the PRODH domain turnover as well as necessary product release steps as shown in Fig. 8. Upon fixing the channeling step rate constant to the value of 0.037 s^{-1} from the single-turnover data, it is obvious that a nonhysteretic mechanism (Fig. 8 with *n* = 1) fails to explain the steady-state data (Fig. 9*A*). In particular, the simulated progress curves rise much more slowly than the experimental steady-state curves (Fig. 9*A*, *inset*).

Next, we fit the single-turnover and steady-state data to a simple hysteretic mechanism in which the rate constant for the channeling step is allowed to vary after the first turnover. The results of fitting the combined data sets to this hysteretic mechanism are shown in Fig. 9 (*B* and *C*). These fits were optimized

with the hysteretic model such that rate constants for steps other than the channeling step were held within a tight range according to already determined confidence intervals. FitSpace calculations (30) for the first turnover (*x* axis in Fig. 9*D*) and subsequent turnovers (*y* axis in Fig. 9*D*) show well constrained best fit values of 0.037 and 1.41 s^{-1}, respectively, for both the first turnover and all subsequent turnovers in the fitting. Confidence intervals for the rate constants are given in Table 3.

EcPutA Multiple-turnover Channeling Experiments—Single-turnover and steady-state PRODH-P5CDH coupled reaction data indicate that *Ec*PutA displays hysteretic behavior in the channeling step. Despite the fact that single-turnover and steady-state data were well fitted to a simple hysteretic model of a single activation event, we were interested in conducting further experiments to test whether stepwise activation of the channeling step occurs in *Ec*PutA PRODH-P5CDH coupled activity. Our strategy was to limit enzyme turnover numbers between one turnover as in single-turnover experiments and >400 turnovers as in steady-state experiments.

WT *Ec*PutA and solutions were made anaerobic to eliminate possible interference by molecular oxygen as an alternative
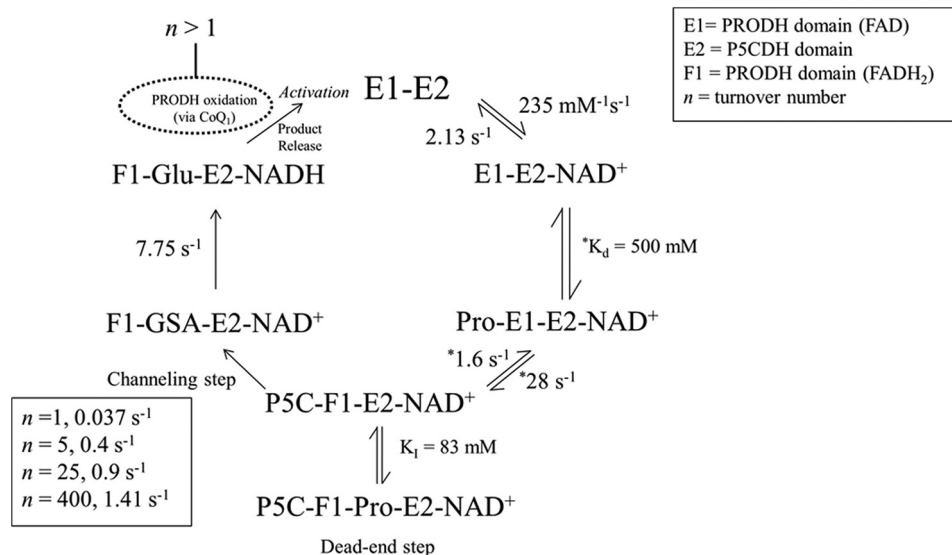
FIGURE 8. Channeling model used for fitting PRODH-P5CDH coupled activity in WT *Ec*PutA with best fit rate constants and equilibrium constants shown for each step. *E1*, oxidized PRODH active site; *E2*, P5CDH active site; *F1*, reduced PRODH active site. The parameter *n* represents the number of catalytic turnovers. Rate constants marked with an *asterisk* were determined in a previous publication (17). A single-turnover experiment is described by this mechanism with $n = 1$ and is performed in the absence of CoQ_1 and O_2 so that the oxidized PRODH active site is not regenerated. The dependence of the channeling rate constant on *n* is determined with defined multiple turnover experiments, which are performed by including CoQ_1 as the limiting reagent at a concentration of $[CoQ_1] = n[EcPutA]$. Confidence intervals for the proposed channeling step through each turnover are given in Table 3.
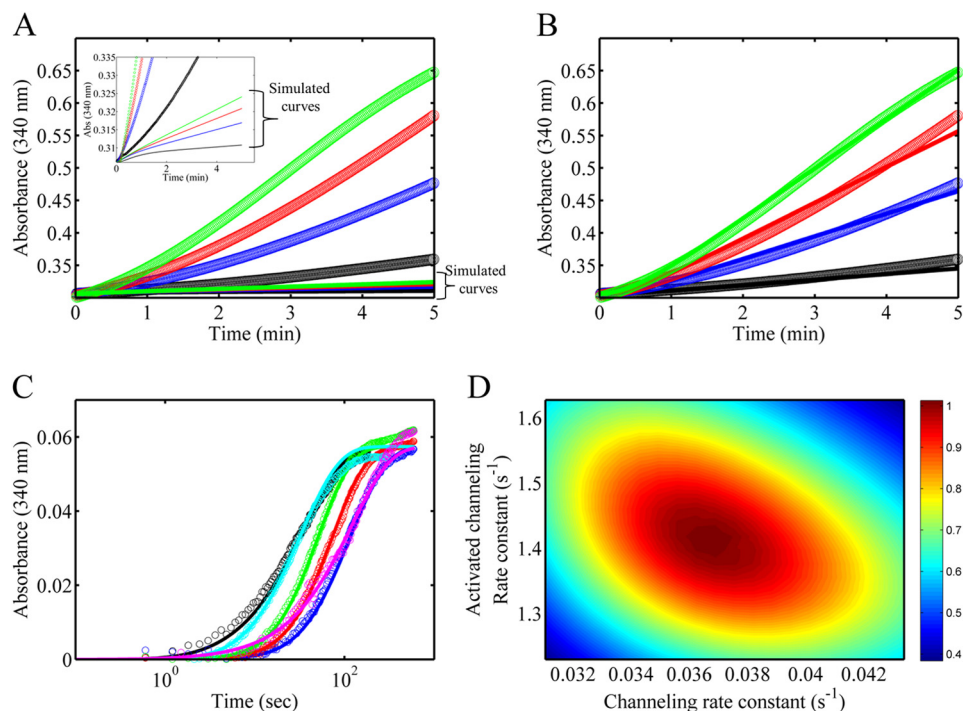

FIGURE 9. Hysteretic behavior of the *Ec*PutA PRODH-P5CDH coupled reaction. *A*, steady-state progress curves of *Ec*PutA (0.5 μM) PRODH-P5CDH coupled activity with 1 mM (*black circles*), 5 mM (*blue circles*), 10 mM (*red circles*), and 20 mM proline (*green circles*) using 0.2 mM NAD^+ and 0.3 mM CoQ_1. Also plotted are the simulated progress *curves* (shown as *solid lines* of the corresponding color) for the steady-state assay conditions using the mechanism in Fig. 8 and a rate constant for the proposed channeling step determined from the *Ec*PutA single-turnover channeling experiment ($n = 1, 0.037\ s^{-1}$). The *inset* shows a zoomed-in view of the large discrepancy between the observed and simulated progress curves. This large discrepancy indicates that the single-turnover channeling rate constant is inconsistent with the steady-state kinetics. *B*, steady-state progress curves as shown in *A* globally fitted to the mechanism shown in Fig. 8 with the rate constant for the channeling step allowed to increase during subsequent enzyme turnovers ($n > 1$). The data are shown as *colored circles*, and the predicted curves are shown as lines colored according to the corresponding data. *C*, *Ec*PutA single-turnover channeling data as shown in Fig. 7*C* but globally fitted here along with the steady-state data in *B* to the mechanism in Fig. 8 allowing for activation of the channeling step. The fitting shows that stopped flow and steady-state data can be reconciled by allowing the rate constant for the proposed channeling step to increase during catalytic cycling. *D*, FitSpace of the global fitting of the steady-state data shown in *B* and the single-turnover data shown in *C* to the model shown in Fig. 8, which includes activation of the proposed channeling step after the first turnover. The effect of varying the channeling rate constant in the first turnover and the activated channeling rate constant in subsequent turnovers on the SSE is shown. Best fit rate constants and confidence intervals are reported in Table 3.

electron acceptor. *Ec*PutA (10 μM) was mixed with 50 μM CoQ$_1$, 200 μM NAD$^+$, and different concentrations of proline (all concentrations after mixing) and followed by multiwavelength absorption (Fig. 10, *A* and *B*). Subsequently, kinetic traces at 340 nm were extracted as shown in Fig. 10*B*. The same experiment except with 2 μM *Ec*PutA was also conducted and is

TABLE 3

Rate constants for the channeling step in the EcPutA PRODH-P5CDH reaction

Turnovers	Channeling step rate constant		
	Best fit value	Lower bound	Upper bound
		s^{-1}	
1 (single-turnover)	0.037	0.033	0.041
5[a]	0.40	0.31	0.53
25[a]	0.90	0.58	2.26
400[a] (steady state)	1.41	1.29	1.54

[a] The number of turnovers is an approximation determined by dividing the limiting CoQ$_1$ concentration by the PutA enzyme concentration.
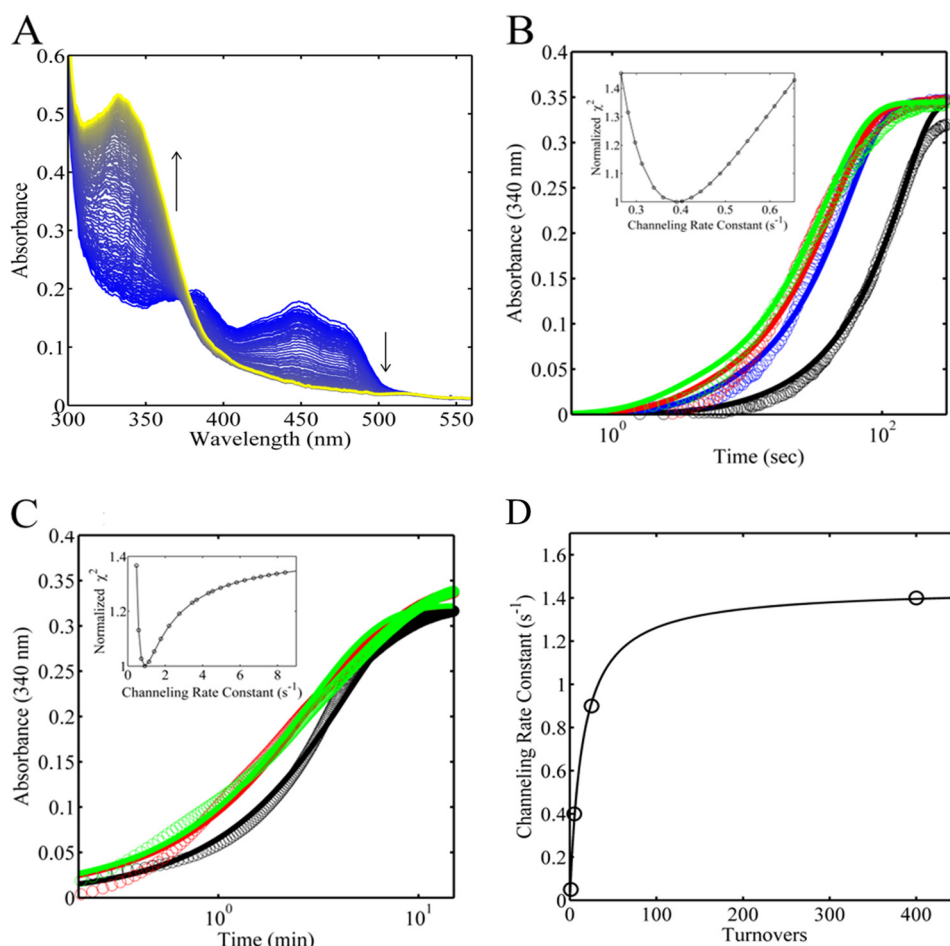
shown in Fig. 10*C*. Each data set was fitted separately to the model shown in Fig. 8 so that the channeling rate constant was allowed to vary, and all other rate constants were only allowed to vary within the previously determined confidence intervals. Best fit channeling rate constants then give the average channeling rate constant over the allotted turnovers.

The data in Fig. 10 (*A* and *B*) were assumed to undergo approximately five turnovers, considering that the limiting reagent concentration (CoQ$_1$ = 50 μM) is five times greater than the enzyme concentration (10 μM). The best fit channeling rate constant for this experiment yielded a value of 0.4 s^{-1}, where the one dimensional FitSpace results are plotted in the *inset* of Fig. 10*B*. Similarly, the data in Fig. 10*C* were assumed to undergo ~25 turnovers because the limiting reagent, CoQ$_1$, was at a concentration 25-fold higher than *Ec*PutA. The best fit channeling rate constant for this experiment yielded a value of 0.9 s^{-1} with the

FIGURE 10. **Anaerobic multiple-turnover experiments of the *Ec*PutA PRODH-P5CDH coupled reaction.** *A*, *Ec*PutA (10 μM) was rapidly mixed with 250 μM NAD$^+$, 50 μM CoQ$_1$, and 10 mM proline (concentrations after mixing), and absorbance changes were monitored with a photodiode array detector. *B*, multi-wavelength data as in *A* were collected with different concentrations of proline 1 (*black*), 5 (*blue*), 10 (*red*), and 25 (*green*) mM (all final concentrations) and analyzed at 340 nm. The data are represented by *colored circles*, and the model predictions are represented by *lines* of the corresponding color. The data were fitted to the mechanism in Fig. 8 that included constrained rate constants for PRODH activity determined previously (17) and P5CDH activity rate constants determined in this study. The *inset* shows the variation of the normalized SSE between the model and the data as the channeling rate constant is varied. *C*, *Ec*PutA (2 μM after mixing) was mixed with 250 μM NAD$^+$, 50 μM CoQ$_1$ with different concentrations of proline 1 (*black*), 5 (*red*), and 10 (*green*) mM (all final concentrations). Single wavelength traces at 340 nm are shown where data are represented by *colored circles*, and the model predictions are represented by *curves* of the corresponding color. These data were fitted to the mechanism in Fig. 8 as described for the data shown in *B*. The *inset* shows the variation of the normalized SSE between the model and the data as the channeling rate constant is varied. *D*, dependence on the channeling rate constant on the number of enzyme turnovers, *n*. The channeling rate constant for *n* = 1 is from the single-turnover experiment shown in Fig. 7. The value for *n* = 400 is from the steady-state data shown in Fig. 9. The values for *n* = 5 and *n* = 25 are from the data shown in *B* and *C*, respectively. For *n* > 1, turnover numbers are estimated by dividing the concentration of the limiting reagent (CoQ$_1$) by the concentration of the enzyme. Fitting to a hyperbola indicates that the channeling rate constant reaches its half-maximal value after 15 turnovers (*n* = 15).
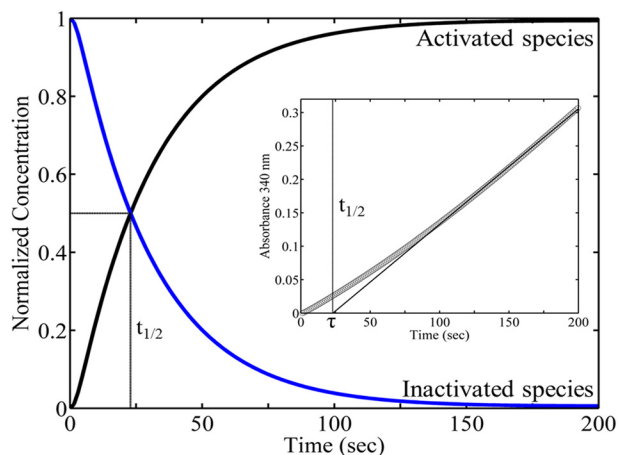
FIGURE 11. **Simulation of the time-dependent activation of the channeling step in *Ec*PutA.** *Ec*PutA PRODH-P5CDH coupled activity was simulated using the rate constants described in this study. The concentrations of activated and inactivated enzyme species in a coupled PRODH-P5CDH assay with 10 mM proline, 0.2 mM NAD^+, and 0.3 mM CoQ_1 are shown as *black* and *blue lines*, respectively (both are normalized by the total enzyme concentration). *Inset*, *Ec*PutA PRODH-P5CDH coupled progress curve data with the same substrate concentrations used for the simulation in the main figure (the progress curve was corrected for CoQ_1 absorbance at 340 nm). The linear portion of the progress curve was fitted to a line and is extrapolated to the *x* axis so that the intersection gives the transient time (τ = 23.47 s) to reach steady state (26, 27). The *black line segments* in the figure mark the $t_{1/2}$ (22.91 s) for activation of *Ec*PutA. Note that the transient time to reach steady state in the coupled PRODH-P5CDH channeling reaction is similar to $t_{1/2}$ for activation of *Ec*PutA.

one-dimensional FitSpace (30) results plotted in the *inset* of Fig. 10C. Confidence intervals are provided in Table 3.

The apparent activation of the channeling step from a single-turnover to steady-state turnover is illustrated by plotting the values of the best fit rate constant for the channeling step *versus* the corresponding turnover number (Fig. 10D). The data in Fig. 10D were fitted to a rectangular hyperbola, which estimates that half-maximum activation of the channeling rate constant is achieved at 15 turnovers (n = 15).

Simulation of Time-dependent Activation of EcPutA Channeling—Additional calculations were conducted to understand the time evolution of *Ec*PutA channeling activation. Simulations were performed to calculate time-dependent changes in the populations of the activated and inactivated enzyme species under the assay conditions (Fig. 11). According to the hysteretic mechanism described above, the population of activated *Ec*PutA rises sharply with full activation at 2 min. The time required to activate half of the total enzyme population ($t_{1/2}$) is estimated to be 22.91 s.

Finally, the NADH progress curve from the experimental data were analyzed by the traditional method of extrapolating the steady-state portion of the trace to the time axis to estimate the transient time, which is the time required to reach steady-state (26, 27). The resulting transient time (τ) is 23.47 s (Fig. 11, *inset*). Interestingly, the $t_{1/2}$ for activation and the transient time have similar values (Fig. 11, *inset*).

DISCUSSION

As a prelude to studying channeling, we determined the kinetic mechanism of the *Ec*PutA P5CDH domain. Although the mechanism of monofunctional human P5CDH has been established (18, 19), ours is the first such study for PutAs.

Steady-state and single-turnover data are consistent with an ordered ternary mechanism (Fig. 5) and suggest that reduction of NAD^+ is the rate-limiting step. This conclusion is corroborated by the fact that single-turnover data should not be limited by product release. As summarized in Table 2, the k_{cat} for the P5CDH reaction using exogenous P5C is nearly identical to the k_{cat} for the PRODH reaction determined previously (16).

The P5CDH kinetic study also established proline as an inhibitor of the PutA P5CDH domain. The K_I of 80 mM proline is much higher than that of monofunctional human P5CDH (K_I = 3 mM) but consistent with the role of proline in osmotic stress. Proline is actively transported into bacterial cells under osmotic stress and accumulates to levels greater than 100 mM. Because this level of proline inhibits PutA P5CDH activity, the PutA-catalyzed conversion of proline to glutamate is down-regulated during osmotic stress. The inhibition of P5CDH activity would also lead to decreased PRODH activity because of the buildup of P5C/GSA, which is a competitive inhibitor of PRODH (K_I = 0.64 mM *versus* proline), in the PutA cavity (16). We note that it is also possible that inhibition of P5CDH would lead to reverse activity; however, the reverse reaction in which PRODH reduces P5C to proline is slow (2.6 M^{-1} s^{-1}) and is not likely to contribute to a rapid accumulation of proline. If the PutA P5CDH domain was inhibited by low millimolar levels of proline, as human P5CDH is, proline catabolism would shut down prematurely, preventing the cell from using proline as a fuel source. Thus, covalently linking PRODH and P5CDH provides an adaptive advantage allowing for simultaneous shutdown of both steps in the proline catabolic pathway to more rapidly accumulate proline during osmotic stress, while allowing flux through the proline catabolic pathway at lower levels of proline.

One of the major outcomes of our work is to show that *Ec*PutA exhibits substrate channeling. Analysis of the rate constants for the PRODH domain described previously (17) and those determined here for the P5CDH domain enabled us to simulate the PRODH-P5CDH coupled reaction of *Ec*PutA. Use of a nonchanneling mechanism (Fig. 6) produces a considerable lag phase on the order of minutes, which is not observed for *Ec*PutA (Fig. 6A). In contrast, the nonchanneling mechanism clearly fits the coupled PRODH-P5CDH activity of the mixed *Ec*PutA variants R556M and C917A (Fig. 6B). These experiments support a channeling mechanism for *Ec*PutA coupled PRODH-P5CDH activity. Kinetic data consistent with substrate channeling have also been reported for PutA from *S. typhimurium* and *Bj*PutA (12, 13). The three channeling PutAs belong to the same branch of the PutA phylogenetic tree (31), suggesting that substrate channeling is a conserved feature of this group of PutAs. Additional kinetic studies will be needed to determine whether channeling is pervasive among PutAs.

Another major result is the discovery of a novel substrate channeling mechanism. Insights into the channeling mechanism of *Ec*PutA were gained by single and multiple turnover experiments of the *Ec*PutA PRODH-P5CDH coupled reaction (Fig. 7). The *Ec*PutA reaction could be well fitted to a minimal model in which a single channeling step was included between the individual PRODH and P5CDH reactions (Fig. 8 with n = 1). Fitting the data to this minimal channeling model gave a well

defined rate constant for this intervening step in the first turnover of 0.033–0.041 s^{-1}, which is about 20-fold slower than k_{cat} (0.73 s^{-1}). This result seems paradoxical, because all forward obligatory rate constants must be greater than or equal to k_{cat} (32, 33). This conundrum was resolved by considering the possibility that the channeling step becomes faster during subsequent turnovers. This assumption seems to describe the data well (Fig. 9, *B* and *C*). Experiments in which 5 and 25 turnovers of *Ec*PutA coupled PRODH-P5CDH activity were conducted and separately fit to the kinetic mechanism in Fig. 8 to estimate the effect of enzyme turnover on the channeling rate constant. Best fit values for the channeling rate constant increased with subsequent turnovers (Fig. 10*D*). From single-turnover to steady-state, the channeling rate constant is estimated to increase 38-fold to a value (1.4 s^{-1}) that is more than k_{cat} (0.73 s^{-1}). The observation that the rate constant for the channeling step increases with catalytic cycling implies that this step of the mechanism is activated.

We used stopped flow kinetics to estimate the number of turnovers required for full activation of the channeling step. The half-maximal increase in the channeling step rate constant occurs at about 15 enzyme turnovers. Simulation of the time-dependent activation of the *Ec*PutA channeling step (Fig. 11) estimates a $t_{1/2}$ of 22.91 s to reach a fully activated channeling enzyme state, which may explain the transient time (23.47 s) observed to reach steady-state formation of NADH.

Over 30 years ago, Frieden conceived the hysteretic enzyme concept to explain enzymes that respond slowly to rapid changes in ligand concentration (28, 29). We suggest that *Ec*PutA is a hysteric enzyme by virtue of the activated channeling step. The half-lives for hysteretic enzymes span from seconds to hours (28). The hysteric step of *Ec*PutA has $t_{1/2}$ of 23 s. Frieden proposed several causes of enzyme hysteresis, including inhibitory ligand displacement, enzyme oligomerization, and isomerization (28). Many enzymes display a hysteretic response (see Table 5 in Ref. 28; see also Refs. 34–39). We are aware of one other hysteretic substrate channeling system, the anthranilate synthase complex from *Bacillus subtilis*, which was observed to display hysteresis during formation of an active complex of the glutamine amidotransferase and the synthase subunits (40, 41). X-ray crystal structures of different glutamine amidotransferases have now shown evidence for conformational changes in both the glutaminase and synthase active sites that enhance activity and help form the ammonia channel (42).

The underlying cause of the observed hysteresis in *Ec*PutA is uncertain. The single-turnover data for PRODH and P5CDH are consistent with steady-state parameters for these individual reactions, whereas the single-turnover rate of the coupled PRODH-P5CDH reaction is significantly slower than the steady-state turnover. This suggests that the observed hysteresis may be associated with the cavity linking the active sites.

One possible cause of hysteresis in *Ec*PutA is that the P5C/GSA generated during the initial turnovers serves to eject solvent out of the cavity to allow efficient movement of P5C/GSA from the PRODH site to the P5CDH site. Analysis of the predicted cavity in the *Ec*PutA model using VOIDOO (reference PMID 15299456) indicates that the cavity volume is in the range of 1500–1700 Å^3. Assuming a molecular volume for P5C/GSA

of 110–130 Å^3, the maximum capacity of the cavity is 12–15 intermediates. Interestingly, half-activation of *Ec*PutA occurs after 15 turnovers. Thus, a potential mechanism of hysteresis may be the filling of the cavity to enhance transport of the P5C/GSA intermediate between the active sites.

Another mechanism of hysteresis may involve conformational changes that optimize the cavity for channeling. Evidence for conformational changes in the PRODH domain have been gleaned from x-ray crystal structures of *Bj*PutA (12), the *Ec*PutA PRODH domain (21, 43, 44), and the monofunctional PRODH enzyme from *Deinococcus radiodurans* R1 (45). Together, these structures show that the conformations of the flavin and surrounding active site residues are highly sensitive to the redox state of the flavin and the occupancy of the proline binding site. The various conformations observed are likely necessary for PRODH catalysis and, in *Ec*PutA, contribute to functional switching. Conformational changes in *Ec*PutA have also been detected by limited proteolysis (46) and rapid reaction kinetics using fluorescence (47) and UV-visible detection (17). These conformational changes are induced by reduction of the FAD cofactor with rates (0.6–2.2 s^{-1}) that are similar to the limiting rate constant (1.4 s^{-1}) observed here for *Ec*PutA PRODH-P5CDH activity. The conformational changes were proposed to be part of the mechanism by which *Ec*PutA switches between DNA binding and membrane binding. From the results here, it appears that conformational changes may also be required to transform *Ec*PutA into a more active enzyme.

How conformational changes would lead to increased channeling activity in *Ec*PutA is not clear but may involve coordination of P5C/GSA release from the PRODH domain into the channel cavity. The x-ray crystal structure of *Bj*PutA shows that the PRODH active site is effectively blocked from the main channel cavity by an ion pair between Arg-456 and Glu-197 (12). These residues are absolutely conserved in PutAs, with the Arg residue being critical for binding the carboxylate moiety of proline (12). It was proposed from the *Bj*PutA structure that the Arg-Glu ion pair breaks during turnover, thus allowing P5C/GSA to be directly released into the channel cavity (12). Because it is a conserved and dynamic component of PRODH active site, the gate could be involved in a conformational change that is required to improve channeling activity in *Ec*PutA. Gating mechanisms are not unusual for channeling enzymes. For example, structural and kinetic analysis of glutamine-dependent NAD$^+$ synthetase identified a gating role for a Tyr residue in the glutaminase active site (48, 49). Tyr-58 is proposed to move and thereby allow ammonia to enter the 40 Å channeling pathway to the NAD$^+$ synthetase active site (48). Molecular dynamics simulations of PutA could provide key insights to help explain our kinetic observations and further test a channel gating hypothesis (12, 20). Other conformational changes not yet known may also contribute to the activation of *Ec*PutA. For instance, in the aldolase-dehydrogenase coupled reaction, conformational changes were found in DmpFG that contribute to allosteric communication and increase channeling activity between the two active sites (50, 51).

Enzyme hysteresis is not only a fascinating biophysical phenomenon, but also a means of metabolic regulation (28). The slow response of an enzyme to a substrate or an allosteric effec-

tor can be used as a metabolite concentration noise filter, which may be crucial to maintain homeostasis inside the cell (28, 52). Thus, a hysteretic enzyme will only commit to sustained changes in the intracellular environment and will be relatively insensitive to short term metabolite fluctuations (39, 52). Here we presented evidence that *Ec*PutA is a hysteretic enzyme in that its channeling rate constant increases ~38-fold from single to steady-state turnover. For future studies, we are interested in determining whether hysteresis occurs in other PutAs, identifying the structural and dynamic basis of PutA hysteresis, and testing the hysteretic effect of *Ec*PutA on the regulation of the *put* operon from a metabolic scale using a systems biology approach (53, 54).

REFERENCES

1. Szabados, L., and Savouré, A. (2010) Proline. A multifunctional amino acid. *Trends Plant Sci.* **15,** 89–97
2. Phang, J. M., Liu, W., and Zabirnyk, O. (2010) Proline metabolism and microenvironmental stress. *Annu. Rev. Nutr.* **30,** 441–463
3. Liang, X., Zhang, L., Natarajan, S. K., and Becker, D. F. (2013) Proline mechanisms of stress survival. *Antioxid. Redox Signal.* **19,** 998–1011
4. Liu, W., Le, A., Hancock, C., Lane, A. N., Dang, C. V., Fan, T. W., and Phang, J. M. (2012) Reprogramming of proline and glutamine metabolism contributes to the proliferative and metabolic responses regulated by oncogenic transcription factor c-MYC. *Proc. Natl. Acad. Sci. U.S.A.* **109,** 8983–8988
5. Natarajan, S. K., Zhu, W., Liang, X., Zhang, L., Demers, A. J., Zimmerman, M. C., Simpson, M. A., and Becker, D. F. (2012) Proline dehydrogenase is essential for proline protection against hydrogen peroxide-induced cell death. *Free Radic. Biol. Med.* **53,** 1181–1191
6. Zarse, K., Schmeisser, S., Groth, M., Priebe, S., Beuster, G., Kuhlow, D., Guthke, R., Platzer, M., Kahn, C. R., and Ristow, M. (2012) Impaired insulin/IGF1 signaling extends life span by promoting mitochondrial L-proline catabolism to induce a transient ROS signal. *Cell Metab.* **15,** 451–465
7. Tanner, J. J. (2008) Structural biology of proline catabolism. *Amino Acids* **35,** 719–730
8. Becker, D. F., Zhu, W., and Moxley, M. A. (2011) Flavin redox switching of protein functions. *Antioxid. Redox Signal.* **14,** 1079–1091
9. Zhou, Y., Larson, J. D., Bottoms, C. A., Arturo, E. C., Henzl, M. T., Jenkins, J. L., Nix, J. C., Becker, D. F., and Tanner, J. J. (2008) Structural basis of the transcriptional regulation of the proline utilization regulon by multifunctional PutA. *J. Mol. Biol.* **381,** 174–188
10. Zhou, Y., Zhu, W., Bellur, P. S., Rewinkel, D., and Becker, D. F. (2008) Direct linking of metabolism and gene expression in the proline utilization A protein from *Escherichia coli*. *Amino Acids* **35,** 711–718
11. Zhu, W., Haile, A. M., Singh, R. K., Larson, J. D., Smithen, D., Chan, J. Y., Tanner, J. J., and Becker, D. F. (2013) Involvement of the β3-α3 loop of the proline dehydrogenase domain in allosteric regulation of membrane association of proline utilization A. *Biochemistry* **52,** 4482–4491
12. Srivastava, D., Schuermann, J. P., White, T. A., Krishnan, N., Sanyal, N., Hura, G. L., Tan, A., Henzl, M. T., Becker, D. F., and Tanner, J. J. (2010) Crystal structure of the bifunctional proline utilization A flavoenzyme from *Bradyrhizobium japonicum*. *Proc. Natl. Acad. Sci. U.S.A.* **107,** 2878–2883
13. Surber, M. W., and Maloy, S. (1998) The PutA protein of *Salmonella typhimurium* catalyzes the two steps of proline degradation via a leaky channel. *Arch. Biochem. Biophys.* **354,** 281–287
14. Ling, M., Allen, S. W., and Wood, J. M. (1994) Sequence analysis identifies the proline dehydrogenase and Δ1-pyrroline-5-carboxylate dehydrogenase domains of the multifunctional *Escherichia coli* PutA protein. *J. Mol. Biol.* **243,** 950–956
15. Arentson, B. W., Sanyal, N., and Becker, D. F. (2012) Substrate channeling in proline metabolism. *Front. Biosci.* **17,** 375–388
16. Moxley, M. A., Tanner, J. J., and Becker, D. F. (2011) Steady-state kinetic mechanism of the proline:ubiquinone oxidoreductase activity of proline utilization A (PutA) from *Escherichia coli*. *Arch. Biochem. Biophys.* **516,** 113–120
17. Moxley, M. A., and Becker, D. F. (2012) Rapid reaction kinetics of proline dehydrogenase in the multifunctional proline utilization A protein. *Biochemistry* **51,** 511–520
18. Forte-McRobbie, C., and Pietruszko, R. (1989) Human glutamic-γ-semialdehyde dehydrogenase. Kinetic mechanism. *Biochem. J.* **261,** 935–943
19. Srivastava, D., Singh, R. K., Moxley, M. A., Henzl, M. T., Becker, D. F., and Tanner, J. J. (2012) The three-dimensional structural basis of type II hyperprolinemia. *J. Mol. Biol.* **420,** 176–189
20. Singh, R. K., Larson, J. D., Zhu, W., Rambo, R. P., Hura, G. L., Becker, D. F., and Tanner, J. J. (2011) Small-angle x-ray scattering studies of the oligomeric state and quaternary structure of the trifunctional proline utilization A (PutA) flavoprotein from *Escherichia coli*. *J. Biol. Chem.* **286,** 43144–43153
21. Zhang, W., Zhang, M., Zhu, W., Zhou, Y., Wanduragala, S., Rewinkel, D., Tanner, J. J., and Becker, D. F. (2007) Redox-induced changes in flavin structure and roles of flavin N_5 and the ribityl 2′-OH group in regulating PutA-membrane binding. *Biochemistry* **46,** 483–491
22. Becker, D. F., and Thomas, E. A. (2001) Redox properties of the PutA protein from *Escherichia coli* and the influence of the flavin redox state on PutA-DNA interactions. *Biochemistry* **40,** 4714–4721
23. Williams, I., and Frank, L. (1975) Improved chemical synthesis and enzymatic assay of delta-1-pyrroline-5-carboxylic acid. *Anal. Biochem.* **64,** 85–97
24. Johnson, K. A., Simpson, Z. B., and Blom, T. (2009) Global kinetic explorer. A new computer program for dynamic simulation and fitting of kinetic data. *Anal. Biochem.* **387,** 20–29
25. Bearne, S. L., and Wolfenden, R. (1995) Glutamate γ-semialdehyde as a natural transition state analogue inhibitor of *Escherichia coli* glucosamine-6-phosphate synthase. *Biochemistry* **34,** 11515–11520
26. Roberts, D. V. (1979) *Enzyme Kinetics*, Cambridge University Press
27. Easterby, J. S. (1973) Coupled enzyme assays. A general expression for the transient. *Biochim. Biophys. Acta* **293,** 552–558
28. Johnson, K. A., Simpson, Z. B., and Blom, T. (2009) FitSpace explorer. An algorithm to evaluate multidimensional parameter space in fitting kinetic data. *Anal. Biochem.* **387,** 30–41
29. Frieden, C. (1970) Kinetic aspects of regulation of metabolic processes. The hysteretic enzyme concept. *J. Biol. Chem.* **245,** 5788–5799
30. Frieden, C. (1979) Slow transitions and hysteretic behavior in enzymes. *Annu. Rev. Biochem.* **48,** 471–489
31. Tanner, J. J., and Becker, D. F. (2013) PutA and proline metabolism. In *Handbook of Flavoproteins* (Hille, R., Miller, S. M., and Palfey, B., eds) pp. 31–56, Walter de Gruyter, Boston
32. Fersht, A. (1985) *Enzyme structure and mechanism*, 2nd Ed., W. H. Freeman, New York
33. Gutfreund, H. (1995) *Kinetics for the Life Sciences: Receptors, Transmitters, and Catalysts*, Cambridge University Press, Cambridge
34. Appleman, J. R., Beard, W. A., Delcamp, T. J., Prendergast, N. J., Freisheim, J. H., and Blakley, R. L. (1989) Atypical transient state kinetics of recombinant human dihydrofolate reductase produced by hysteretic behavior. Comparison with dihydrofolate reductases from other sources. *J. Biol. Chem.* **264,** 2625–2633
35. Mather, M. W., and Gennis, R. B. (1985) Kinetic studies of the lipid-activated pyruvate oxidase flavoprotein of *Escherichia coli*. *J. Biol. Chem.* **260,** 16148–16155
36. Powlowski, J. B., Dagley, S., Massey, V., and Ballou, D. P. (1987) Properties of anthranilate hydroxylase (deaminating), a flavoprotein from *Trichosporon cutaneum*. *J. Biol. Chem.* **262,** 69–74
37. Sümegi, B., Batke, J., and Porpáczy, Z. (1985) Substrate-induced structural changes of the pyruvate dehydrogenase multienzyme complex. *Arch. Biochem. Biophys.* **236,** 741–752
38. Jiménez, M., and García-Carmona, F. (1996) Kinetics of the slow pH-mediated transition of polyphenol oxidase. *Arch. Biochem. Biophys.* **331,** 15–22
39. Kadirvelraj, R., Sennett, N. C., Custer, G. S., Phillips, R. S., and Wood, Z. A. (2013) Hysteresis and negative cooperativity in human UDP-glucose dehydrogenase. *Biochemistry* **52,** 1456–1465
40. Holmes, W. M., and Kane, J. F. (1975) Anthranilate synthase from *Bacillus subtilis*. The role of a reduced subunit X in aggregate formation and amidotransferase activity. *J. Biol. Chem.* **250,** 4462–4469

41. Kane, J. F., Homes, W. M., Smiley, K. L., Jr., and Jensen, R. A. (1973) Rapid regulation of an anthranilate synthase aggregate by hysteresis. *J. Bacteriol.* **113,** 224–232

42. Mouilleron, S., and Golinelli-Pimpaneau, B. (2007) Conformational changes in ammonia-channeling glutamine amidotransferases. *Curr. Opin. Struct. Biol.* **17,** 653–664

43. Lee, Y. H., Nadaraia, S., Gu, D., Becker, D. F., and Tanner, J. J. (2003) Structure of the proline dehydrogenase domain of the multifunctional PutA flavoprotein. *Nat. Struct. Biol.* **10,** 109–114

44. Srivastava, D., Zhu, W., Johnson, W. H., Jr., Whitman, C. P., Becker, D. F., and Tanner, J. J. (2010) The structure of the proline utilization a proline dehydrogenase domain inactivated by *N*-propargylglycine provides insight into conformational changes induced by substrate binding and flavin reduction. *Biochemistry* **49,** 560–569

45. Luo, M., Arentson, B. W., Srivastava, D., Becker, D. F., and Tanner, J. J. (2012) Crystal structures and kinetics of monofunctional proline dehydrogenase provide insight into substrate recognition and conformational changes associated with flavin reduction and product release. *Biochemistry* **51,** 10099–10108

46. Zhu, W., and Becker, D. F. (2003) Flavin redox state triggers conformational changes in the PutA protein from *Escherichia coli*. *Biochemistry* **42,** 5469–5477

47. Zhu, W., and Becker, D. F. (2005) Exploring the proline-dependent conformational change in the multifunctional PutA flavoprotein by tryptophan fluorescence spectroscopy. *Biochemistry* **44,** 12297–12306

48. Chuenchor, W., Doukov, T. I., Resto, M., Chang, A., and Gerratana, B. (2012) Regulation of the intersubunit ammonia tunnel in *Mycobacterium tuberculosis* glutamine-dependent NAD+ synthetase. *Biochem. J.* **443,** 417–426

49. LaRonde-LeBlanc, N., Resto, M., and Gerratana, B. (2009) Regulation of active site coupling in glutamine-dependent NAD$^+$ synthetase. *Nat. Struct. Biol.* **16,** 421–429

50. Smith, N. E., Tie, W. J., Flematti, G. R., Stubbs, K. A., Corry, B., Attwood, P. V., and Vrielink, A. (2013) Mechanism of the dehydrogenase reaction of DmpFG and analysis of inter-subunit channeling efficiency and thermodynamic parameters in the overall reaction. *Int. J. Biochem. Cell Biol.* **45,** 1878–1885

51. Smith, N. E., Vrielink, A., Attwood, P. V., and Corry, B. (2012) Biological channeling of a reactive intermediate in the bifunctional enzyme DmpFG. *Biophys. J.* **102,** 868–877

52. Wu, Z., and Xing, J. (2012) Functional roles of slow enzyme conformational changes in network dynamics. *Biophys. J.* **103,** 1052–1059

53. Dexter, J. P., and Gunawardena, J. (2013) Dimerization and bifunctionality confer robustness to the isocitrate dehydrogenase regulatory system in *Escherichia coli*. *J. Biol. Chem.* **288,** 5770–5778

54. Beard, D. A., and Qian, H. (2008) *Chemical Biophysics: Quantitative Analysis of Cellular Systems*, Cambridge University Press, Cambridge

55. Johnson, K. A. (1986) Rapid kinetic analysis of mechanochemical adenosinetriphosphatases. *Methods Enzymol.* **134,** 677–705